Journal of Network Intelligence
Taiwan Ubiquitous Information
 ISSN 2414-8105 (Online)
Volume **9**, Number **2**, May **2024**

Non-Intrusive Load Event Identification Algorithm Based on Color Coding

Wen-Yu Hu*

College of Computer Science and Mathematics
Fujian Provincial Key Laboratory of Big Data Mining and Applications
Fujian University of Technology
Xuefu South Road, Fuzhou City, Fujian Province, 350118, China
493234029@qq.com

Guo-Nong Li

College of Computer Science and Mathematics
Fujian Provincial Key Laboratory of Big Data Mining and Applications
Fujian University of Technology
Xuefu South Road, Fuzhou City, Fujian Province, 350118, China
Liiguonong@gmail.com

*Corresponding author: Wen-Yu Hu

Received May 7, 2023, revised August 1, 2023, accepted November 24, 2023.

Abstract. *Non-invasive load monitoring (NILM) can help residents monitor the operation of household appliances and achieve the purpose of energy conservation and emission reduction. Load event identification is a key task of non-intrusive load monitoring. In order to enrich the characteristics of load events and improve the identification accuracy of load events, a load event identification algorithm based on color coding (CCA) is proposed. On the basis of retaining the basic waveform of active power, the three characteristics of active power (R), reactive power (G) and reactive power change trend (B) are fused to construct the color image of load events, and the image is trained and recognized based on the AlexNet convolutional neural network with parameter adjustment. The experimental results show that this load event identification algorithm can stably and effectively distinguish the load events of different devices. Compared with three commonly used classifiers, the results show that this algorithm is superior to the traditional event classification algorithm based on power sequence.*
Keywords: Non-invasive load monitoring, load event identification, feature extraction, color code

1. **Introduction.** Energy crisis and climate change are two major challenges facing the world today [1]. Improving energy consumption structure to reduce fossil energy demand is the key measure to deal with these two challenges. With the improvement of living standards of Chinese residents, the proportion of household electricity consumption in the total electricity consumption of the national economy is increasing. Non-intrusive load monitoring (NILM) [2] analyzes the overall power consumption data of a household to enable operation monitoring and energy consumption analysis of various electrical appliances within the home. This is beneficial for users to timely and comprehensively understand the usage patterns of different electrical appliances, optimize the structure of electricity consumption, and achieve the goal of energy saving and emission reduction. With the development of deep learning algorithms [3], optimization algorithms [4, 5, 6],

and cloud computing [7] , and the popularization of smart grids [8, 9], NILM has begun to receive widespread attention from engineering and academia. In NILM, an event is a switch in the operating status of an electrical appliance [10]. NILM can be divided into event-based and event-free schemes depending on whether load events need to be detected or not [11]. Event detection and load event identification are two important tasks of event-based NILM. The research in this paper focuses on load event identification.

The active power curve, also called the waveform of active power, reflects the energy consumption information and operating state of the system. Afzalan et al. [12] designed a self-configured event detection algorithm using active power waveform clustering. Xiao et al. [13] achieved load event identification by fitting active power curves with an improved KM algorithm. Image processing techniques and feature construction techniques are widely used in practical engineering [14]. Constructing load characteristic models through color coding has been a current research hot topic in NILM. Cui et al. [15] propose a true-color feature image where the red-green-blue (RGB) values are converted by the voltage, current, and V-I_f trajectory information of the loads. In Ding et al. [16], the active current of the loads, the slope of the straight line segment between the adjacent sampling points of the V-I_f trajectory, and the average instantaneous power of adjacent sampling points are extracted as the RGB values.

Based on the above research, a non-intrusive load event identification algorithm based on RGB color coding (CCA) is proposed. The overall process is shown in Figure 1. The active power load curve is mapped to a 5×5 RGB image, using active power as the R-channel, reactive power as the G-channel, and the waveform change of reactive power as the B-channel. This algorithm fuses the numerical features of load events with image features to contain richer electrical information. The uniqueness of load characteristics is enhanced and power consumption and energy exchange during equipment operation are better reflected by the color image. More accurate differentiation between different operating states of various equipment can be achieved by using color images in load event identification. Based on color image feature data, AlexNet convolutional neural network [17] is used for model training and event recognition.

2. **Load event feature extraction based on color coding.**

2.1. **Mapping rules for color images.**

Resistive, inductive and capacitive loads are the main types of loads in an electrical circuit [18]. There are some differences in their transient processes. For purely resistive loads, the current response in the circuit is instantaneous when the device is turned on or off, and the current magnitude is controlled by Ohm's law without any transient process. The duration of load events for purely resistive loads is extremely short, usually lasting only a few milliseconds. For inductive loads, the current in the circuit changes slowly as the inductance blocks the current when the device is turned on or off. When an inductive load is turned on and off, there is a rise or fall of current in the circuit until steady state is reached. The duration of load events for inductive loads depends on the inductance and load resistance values in the circuit and can range from a few hundred milliseconds to a few seconds or even longer [19]. For capacitive loads, the transient response is usually very short, usually lasting only a few milliseconds or less [20], because the capacitor can charge and discharge very quickly.

To capture more event characteristics of inductive loads, the algorithm selects 100 active and reactive power data points with a sampling frequency of 60Hz at and after the point of event occurrence, which are then divided into five equal parts to build a 5×5 RGB matrix:

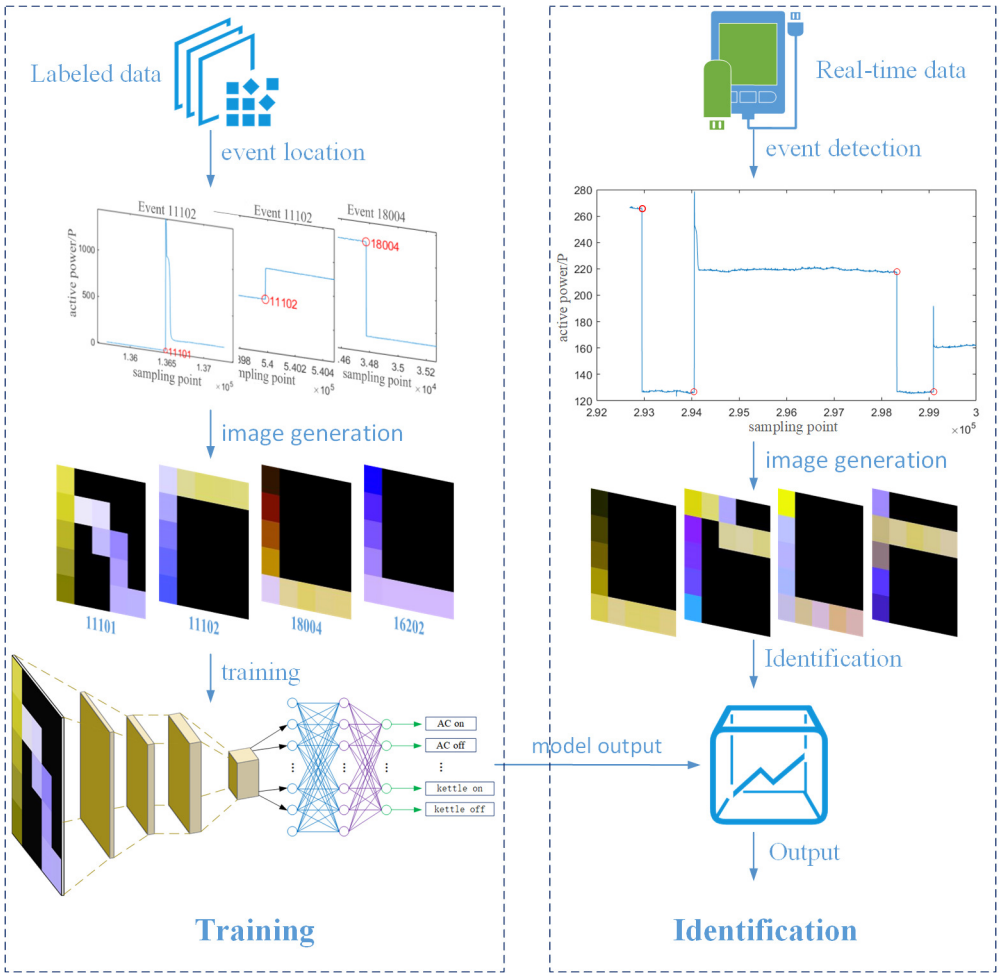

FIGURE 1. The overall flow chart of this algorithm

(1) Assume that the active power set and the reactive power set containing 100 sampled data:

$$P = \{p_i \mid i = 1, 2, ..., 100\} = \bigcup_{t=1}^{5} P_t = \bigcup_{t=1}^{5} \{p_i \mid i \in [20(t-1)+1, 20t]\} \tag{1}$$

$$Q = \{q_i \mid i = 1, 2, ..., 100\} = \bigcup_{t=1}^{5} Q_t = \bigcup_{t=1}^{5} \{q_i \mid i \in [20(t-1)+1, 20t]\} \tag{2}$$

where, P, Q is the total data set, p_i, q_i is the $i-th$ sampled data, andP_t, Q_t is the data set of the $t-th$ time span.

(2) The resolution of the image is 5×5. Using time t as the horizontal axis and active power P as the vertical axis, all sample points are mapped onto the grid with the dimensions of each pixel:

$$\begin{cases} \Delta t = \dfrac{100}{5} = 20 \\ \Delta p = \dfrac{p_{\max} - p_{\min}}{5} \end{cases} \tag{3}$$

where, p_{max}, p_{min} is the maximum and minimum values of the 100 active power sampling data, Δt is the cell horizontal coordinate size, Δp is the cell vertical coordinate size.

(3)The mapping coordinates of the sample points are determined via:

$$(x,y)=\begin{cases} x=\left\lceil \dfrac{i}{\Delta t}\right\rceil \\ y=\left\lceil \dfrac{p_i-p_{\min}}{\Delta P}\right\rceil \end{cases} \tag{4}$$

where, $\lceil\rceil$ represents rounding up.

2.2. **Color coding algorithm.** (1) R-channel

In a power system, when an event occurs, the power change is relative to the base load, but the active power recorded by the measuring device is an absolute value. Therefore, before calculating the active power statistics of the event, it is necessary to obtain the relative value of the active power of the event. In this paper, the difference between the sampling point and its minimum value is the relative value of the power, that is $p_i - p_{min}$.

Firstly, the cumulative sum of the relative values of the active power of 100 sampling points is obtained as the denominator, and then the cumulative sum of the relative values of the active power in each time span is obtained as the molecule. The logarithm of the numerator and denominator is taken, and the ratio is taken as the value of the R-channel at the position, see Equation (5). The logarithm operation is to normalize the data, and the independent variable of the logarithmic function is added by 1 to ensure that the final value is positive. Because the value range of RGB coding is [0,255], the final result needs to be multiplied by 255.

$$R(x,y)=255\frac{\lg\left[1+\sum_{i=P_t}\left(p_i-p_{\min}\right)\right]}{\lg\left[1+\sum_{i=P}\left(p_i-p_{\min}\right)\right]} \tag{5}$$

(2) G-channel

The G-channel uses reactive power as the original data, and its construction process is the same as the R-channel:

$$G(x,y)=255\frac{\lg\left[1+\sum_{i=Q_t}\left(q_i-q_{\min}\right)\right]}{\lg\left[1+\sum_{i=Q}\left(q_i-q_{\min}\right)\right]} \tag{6}$$

(3) B-channel

There will be a problem in using the above scheme to construct R-channel and G-channel, $p_i - p_{min}$ and $q_i - q_{min}$ only consider the amplitude of active and reactive power, ignoring the trend of active and reactive power. For two load events with similar magnitude of power change before and after the event, but with different trends, the values of their R and G channels may not differ much, affecting the final classification effect.

Figure 2 shows the comparison of two similar events. The change in active power for event 1 is 2000W with a step-up trend (top left), and the change in reactive power is 100Var with a step-down trend (bottom left). The change in active power for event 2 is 1800W with a step-up trend (top right) and the change in reactive power is 90Var with a step-up trend (bottom right). Figure 3 shows the color images constructed by using only the R and G channels for the two events. It can be seen that the two images have same shape and similar tones.

Because the shape of the color image represents the trend of active power, only the trend of reactive power is considered in constructing the B-channel. To obtain the trend of the reactive power, the rising statistic T_{up} and the falling statistic T_{down} are defined and their values are calculated in Equation (7). The ratio of the rise statistic T_{up} to the total change $(T_{up} + T_{sown})$ is used to quantify the extent of the rising trend in reactive power. The value of the B-channel is determined by Equation (8).

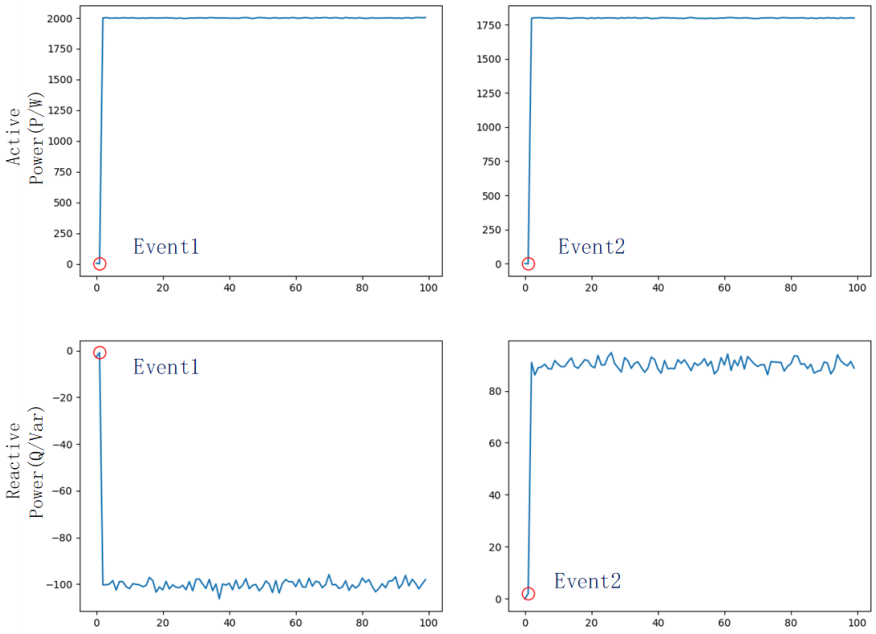

FIGURE 2. Comparison of two similar events

FIGURE 3. Color images constructed by two channels

$$\begin{cases} T_{\text{up}} = \sum |q_i - q_{i-1}| & , q_i - q_{i-1} \geq 0 \\ T_{\text{down}} = \sum |q_i - q_{i-1}| & , q_i - q_{i-1} < 0 \end{cases} \tag{7}$$

$$B(x, y) = 255 \frac{T_{up}}{T_{up} + T_{\text{down}}} \tag{8}$$

Encoding of event 1 and event 2 using RGB triple channel, their feature image is shown in Figure 4. It can be seen that the tonal difference between the two images is obvious and can satisfy the requirement of distinguishing the two events. When event 2 occurs, the rising trend of reactive power is obvious, corresponding to a value of 225-255 for the B-channel, indicating that the ratio of the rising statistics to the total change is large, so this part of the pixel shows a blue tone. After the end of the rise, the reactive power waveform is flat and fluctuates up and down only by the influence of electrical noise, which corresponds to a value of 120-135 for the B-channel, indicating that the rising and falling statistics have basically the same proportion, each accounting for half of the total variation. When event 1 occurs, the downward trend of the reactive power is obvious and it takes a small value for the B-channel, so that this part of the pixel point does not show a blue tone.

2.3. **Event color images of EMBED.** EMBED was collected by Jazizadeh et al. [21], contains 14-27 day total load data and marker event data for three U.S. residences. To further verify the feasibility of color image features for distinguishing different events,

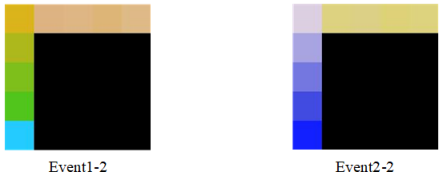

FIGURE 4. Color images encoded by RGB

color images of 24 types of load events selected from the EMBED dataset are plotted. Figure 5 shows the active power waveforms of the events and Figure 6 shows the color image features of the events.

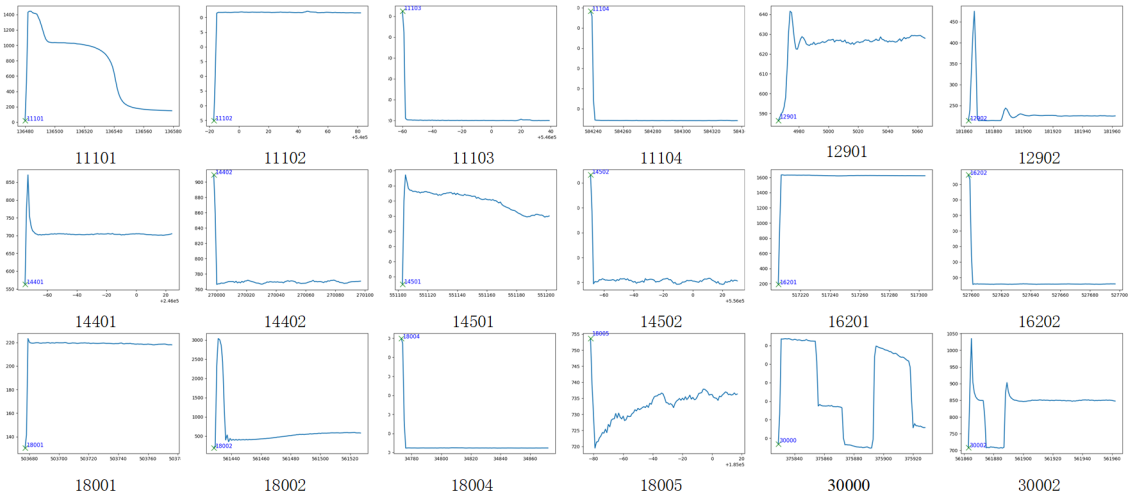

FIGURE 5. Active power waveforms of events

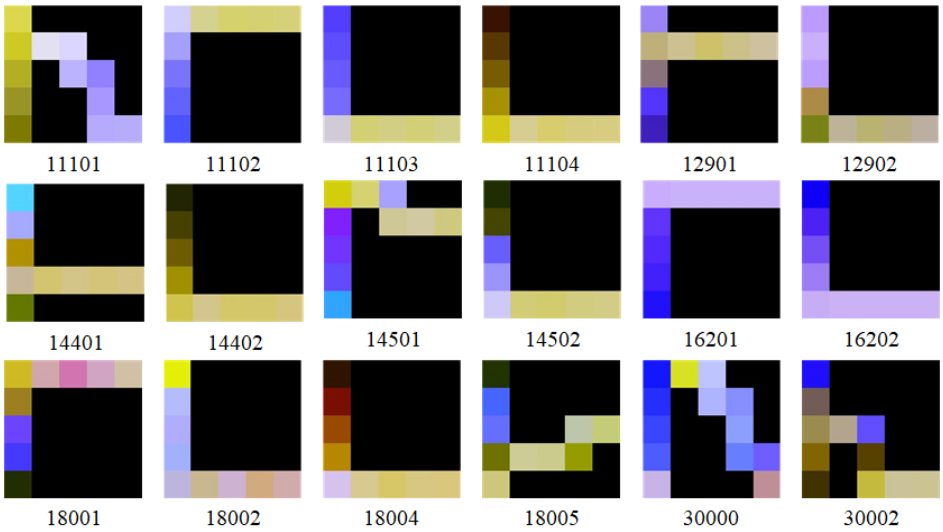

FIGURE 6. Color images of events

It can be seen that the color image with RGB encoding preserves the basic shape of the active power waveform and the color scheme of different events is recognizable. For images

with similar shapes, such as 11102, 16201 and 18001, different events can be identified by color. For images with similar color schemes, such as 16201, 16202 and events 11102 and 11103, which are generally switching events of the same device, it is possible to identify the different events by their shapes. For some events with pulse durations shorter than 20 sampling points, such as 12902 and 18002, their spike waveforms will be drowned out, but the spike waveform characteristics can still be reflected by color, so it has little impact on the classification of events. Due to the limited number of pixel points, for the very few events with complex transient processes, such as 30000, the retained basic waveforms are not complete enough, which may affect the classification effect.

Overall, the constructed color images meet the design expectations and reflect a large variation in waveform retention and color matching, which can be used as features to distinguish different events.

3. **AlexNet-based load event identification algorithm.** Deep learning algorithms have been used quite extensively in the field of image classification [22]. In this paper, we use AlexNet convolutional neural network to recognize color images of load events.

3.1. **Structure of AlexNet.** AlexNet is a large, multi-layer convolutional neural network algorithm [17], and its basic structure is shown in Table 1. The algorithm consists of approximately 60 million parameters and 650,000 neurons, which are divided into 8 layers, with the first 5 layers being convolutional layers.

Table 1. Structure of AlexNet

No.	Layer Type	Output Size	Filter Size	Activation Function
0	Input	$224 \times 224 \times 3$	—	—
1	Convolution	$55 \times 55 \times 96$	$11 \times 11 \times 3 \times 96$	ReLU
	Pooling	$27 \times 27 \times 96$	3×3	—
2	Convolution	$27 \times 27 \times 256$	$5 \times 5 \times 96 \times 256$	ReLU
	Pooling	$13 \times 13 \times 256$	3×3	—
3	Convolution	$13 \times 13 \times 384$	$3 \times 3 \times 256 \times 384$	ReLU
4	Convolution	$13 \times 13 \times 384$	$3 \times 3 \times 384 \times 384$	ReLU
5	Convolution	$13 \times 13 \times 256$	$3 \times 3 \times 384 \times 256$	ReLU
	Pooling	$6 \times 6 \times 256$	3×3	—
6	Fully Connected	4096	—	ReLU
7	Fully Connected	4096	—	ReLU
8	Fully Connected	1000	—	Softmax

AlexNet introduces several techniques to improve the accuracy of image classification. For example, using ReLU as the activation function of CNN solves the problem of gradient disappearance of traditional activation function; using overlapping maximum pooling enhances the feature richness; introducing Dropout to randomly discard some neurons during training to avoid model overfitting. In addition, it employs GPU parallel computing to accelerate the training and inference of the model, allowing a good balance between training time and accuracy.

3.2. **AlexNet parameter setting.** The color image feature of the load event is a 5×5 image, which is incompatible with the default input size of AlexNet. In order to enable AlexNet to recognize feature images, several approaches are taken to modify AlexNet to improve classification. Figure 7 (right) shows the sketch of the improved structure.

(1) Convolution kernel size and number: The size and number of convolution kernels affect the generalization ability of the model [23]. Since the feature data of small images

is more concentrated, the convolution kernel is required to capture more detailed features, so a smaller size convolution kernel can be selected. Fewer convolution kernels may cause information loss and underfitting, and more convolution kernels may cause overfitting. The size of the input image in this example is small and the sample size is not sufficient, so the number of convolution kernels can be reduced to avoid over-fitting of the model. The size of the convolution kernel of the first convolution layer is adjusted from 11×11×3 to 3×3×3, and the number of filters is reduced from 96 to 32. The convolution kernels of the subsequent four convolution layers are also adjusted to 3×3×3, and the number of filters are adjusted to 64, 128, 256, 256, respectively.

(2) Size of pooling kernel: A smaller pooling kernel can avoid losing too much information during the pooling process [24], but it will increase the processing time and affect the operating efficiency of the model. Because the size of the constructed feature image is only 5×5, the efficiency drop caused by appropriately reducing the size of the pooling kernel is within an acceptable range. So in this model, the pooling kernel size of each max pooling layer is adjusted from 3×3 to 2×2.

(3) Size of the fully connected layer: The smaller size of fully connected layers can prevent overfitting [25], improve the training speed, and optimize the performance and efficiency of the model. So in this model, the output dimension of the first two fully connected layers is adjusted from 4096 to 1024, and the output dimension of the last connected layer is adjusted to the number of event labels 42.

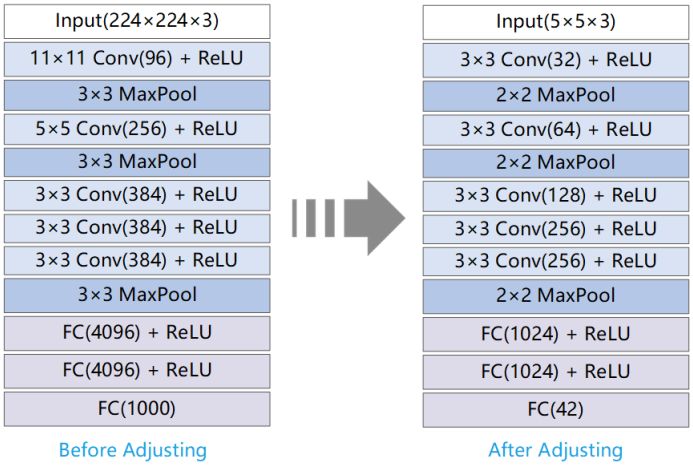

FIGURE 7. Sketch of AlexNet structure

3.3. **Training process.** The cross-entropy function is chosen as the minimum loss function, the optimization algorithm is adaptive moment estimation, the learning rate is 1.0×10^{-3}, the discard rate is 0.2, and the number of batches is 100. The specific training steps are as follows.

(1) Load the pre-trained AlexNet model and reconfigure its output neurons according to the number of load event categories.

(2) Use the proposed algorithm to construct the color image data set of load events and divide the data set into test set and training set.

(3) Input the labeled training set into the AlexNet model for supervised learning until the termination conditions are met.

(4) Use the test set to verify the identification ability of the algorithm.

4. Experiment and performance analysis.

Table 2. Sample size of training and test

Label	Composition	Label	Composition	Label	Composition
11101	304/77	14001	362/91	16201	36/9
11102	88/23	14002	355/89	16202	38/10
11103	211/53	14401	74/20	18001	98/25
11104	88/23	14402	76/20	18002	139/35
12901	33/9	14501	338/85	18004	144/36
12902	72/18	14502	331/83	30000	249/63

4.1. **Experimental data.** Use the A-phase data of apartment 1 in EMBED, which has 42 types of event tags and 1699 tagged events, to test the proposed load event identification algorithm.

The number of samples of various load events in the EMBED data set varies greatly. Some events have only single-digit labeled samples, which easily leads to low identification effect of some events. Therefore, only 18 event types with more labeled data are selected for model training and testing. Since the time point detected by the event detector does not always fall on the power change point, in order to increase the generalization ability of the model and expand the training data size, each marker event is moved five sampling points to the left and five sampling points to the right to construct new marker data and expand the number of marker events.

Use the proposed algorithm to construct the color image data set of load events. Divide the data set into test set and training set at a ratio of 8:2 by stratified sampling. The divided training set contains 18 event labels for a total of 3036 labeled event images, and the test set contains 18 event labels for a total of 769 labeled event images. The number of samples for each event label is shown in Table 2.

4.2. **Parametric optimization.** In order to quantitatively analyze the influence of training times on the algorithm performance, the curve of identification accuracy and loss value with the number of training times in the training process is drawn, as shown in Figure 8. The whole test takes about 2.5h and the number of epochs is 120. It can be seen that in the early stage of calculation, with the increase of training times, the loss function value decreases continuously, and the identification accuracy of the test set increases rapidly. When the number of training times reaches about 20 times, the identification accuracy has exceeded 90%, and it begins to increase slowly in subsequent training. When the number of training reaches 100 times, the accuracy of both the loss function and the test set tends to be stable, and the classification performance of the algorithm will not change much. Based on the above analysis, the training times are set to 100 times, and a satisfactory identification effect can be obtained in a relatively short time.

4.3. **Analysis of identification results.** The 769 labeled event images containing 18 event types were input to the model for testing, and Table 3 shows the Precision, Recall and F_1-Score for each event label. Because the number of test samples for each event is different, in order to better evaluate the identification effect of the model on different events, the final result is standardized as a confusion matrix with 50 samples per event. and Figure 7 shows the normalized confusion matrix of the test results.

In terms of Precision [26], all events except event 14402 exceeded 81%, and seven events reached 100% Precision. From Table 3, it can be seen that 14402 is a load event triggered by the bedroom lamp, and its power is small and similar to that of other lamps, so it is presumed that the main factor affecting Precision of event 14402 is the misidentification

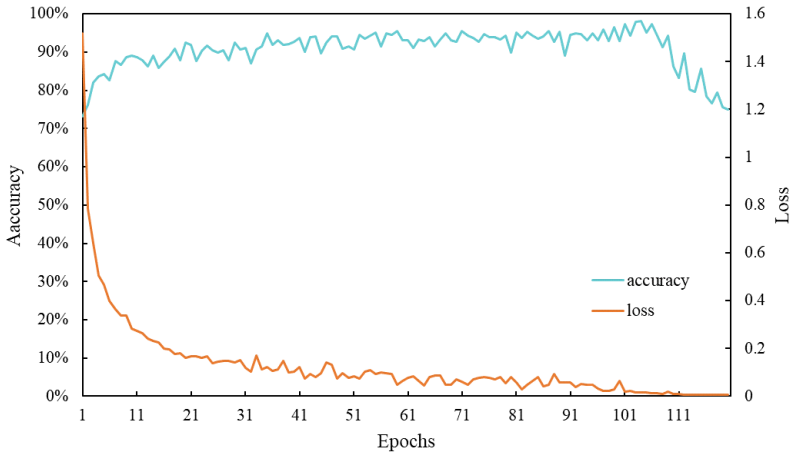

FIGURE 8. Influence of training times on algorithm performance

TABLE 3. Event identification test results

Label	Precision	Recall	F_1-Score	Label	Precision	Recall	F_1-Score
11101	100%	98.70%	99.35%	14402	52.94%	90%	66.67%
11102	100%	100%	100.00%	14501	97.70%	100%	98.84%
11103	98.04%	94.34%	96.15%	14502	84.95%	95.18%	89.77%
11104	81.48%	95.65%	88%	16201	100%	100%	100.00%
12901	100%	100%	100%	16202	100%	90%	94.74%
12902	94.44%	94.44%	94.44%	18001	100%	100%	100%
14001	98.85%	94.51%	96.63%	18002	97.14%	97.14%	97.14%
14002	86.81%	90%	88.38%	18004	100%	100%	100.00%
14401	86.36%	95%	90.47%	30000	94.87%	58.73%	72.55%

of other lamp events. From the confusion matrix, the events misidentified as 14402 are mainly 14002, 14502 and 30000, where 140 and 145 are the labels of luminaire devices, and 300 is the label of multiple unknown devices, which may contain some untagged luminaires, thus confirming the validity of the previous speculation.

In terms of Recall, all events except event 30000 have a Recall of over 90%, and six events have a Recall of 100%. Since event 30000 contains multiple unknown devices, the main factor affecting its Recall is that its feature image contains multiple different waveforms and multiple different color schemes, which leads to the lack of obvious features of the trained model. From the confusion matrix, event 30000 is mainly misidentified by the loading events of the lamps, indicating that event 30000 contains untagged lamps with high probability.

In terms of F_1-Scores, all events scored over 88%, except for event 14402 and event 30000, which scored lower. This is due to the lower precision of event 14402 and the lower recall of event 30000, pulling down the corresponding F_1-Scores.

Comprehensive three dimensions. For devices with high power, color image features can well distinguish load events between them. For individual low load events, there is still room for improvement in the identification accuracy of color image features. The load event color image constructed based on RGB coding achieves stable and effective identification effect in most test cases, which proves that this algorithm can be used to distinguish load events of different devices.

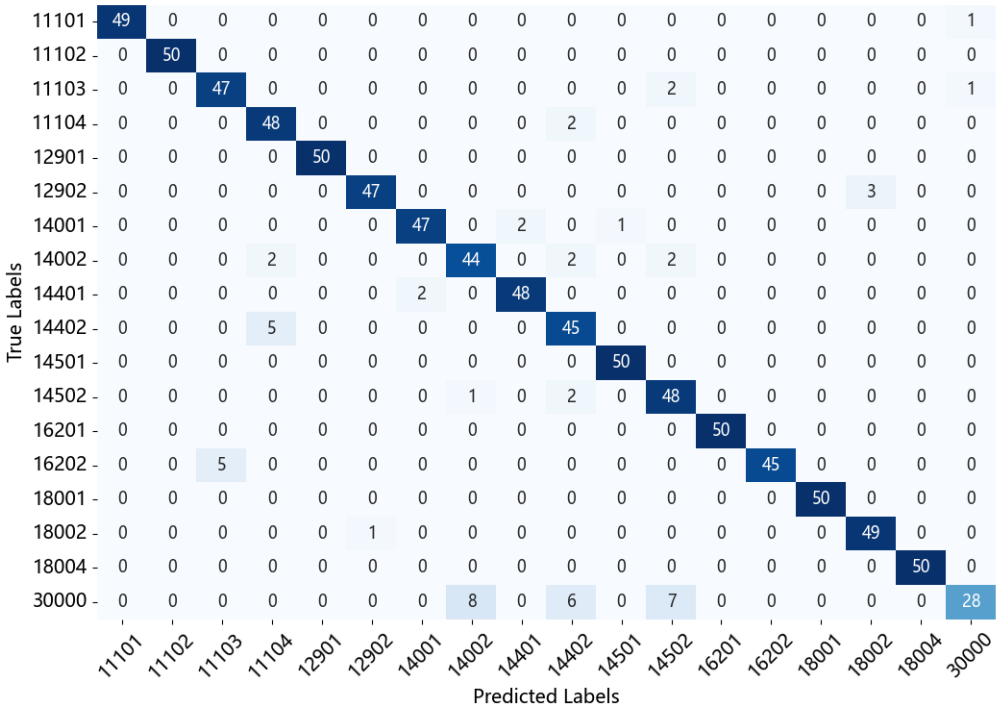

FIGURE 9. Standardized confusion matrix of test results

TABLE 4. Comparison of identification results of different algorithms

Algorithm	Precision	Recall	F_1-Score
CCA	93.66%	92.72%	93.19%
KNN	89.58%	91.68%	90.62%
NBC	85.71%	76.46%	80.82%
SVM	52.68%	69.57%	59.96%

4.4. **Comparison of different algorithms.** In order to further verify the effectiveness of the algorithm based on color coding, based on the experimental data in Table 2, 50 sets of active power and reactive power sample points before and after each labeled event are taken as input. K-Nearest Neighbor (KNN) [27], Naive Bayes Classifier (NBC) [28] and Support Vector Machine (SVM) [29, 30], which are three classifiers commonly used in the field of non-intrusive load monitoring, are used to train and classify the marked events. The specific results of the experiment are shown in Table 4.

It can be seen from the comparison data that the load identification algorithm proposed in this paper has the best performance, followed by KNN and NBC, and SVM has the worst performance. Compared with the traditional classification algorithm that directly learns the combination sequence of active power and reactive power, the algorithm proposed in this paper is improved from two aspects : feature construction and model training. The RGB color coding principle is used to realize the extraction and fusion of four-dimensional features of active power, reactive power, active power waveform and reactive power change trend, which significantly improves the feature difference between different events and enhances the identification ability of the algorithm.

5. **Conclusions.** The goal of load event identification is to identify the type of load events by extracting various types of characteristics of device events through various algorithms and then matching them with the event model in the database. The accurately identified load events can be used to achieve energy consumption monitoring of devices. They can also be used for intelligent control of homes and fault detection of hardware. In order to improve the identification accuracy of load events, we propose a feature construction algorithm of load events based on RGB coding: the active power load curve is mapped onto a 5×5 RGB image, the active power is selected as the R-channel, the reactive power as the G-channel, and the change trend of reactive power as the B-channel, and the color image features of load events are constructed, so as to improve the informativeness of load events.

Color images are constructed using EMBED's labeled events, and the images are trained and recognized based on the improved AlexNet. The experimental results show that the load event feature is able to distinguish load events of different devices stably and effectively. KNN, NBC and SVM classifiers are used to compare with this algorithm. The results show that the algorithm is superior to the traditional event classification algorithm based on power sequence.

Acknowledgment. The authors gratefully acknowledge the financial support provided by Sub-project of National Key R&D Program(2018Y*C12***03).

REFERENCES

[1] G. D. Valasai, M. A. Uqaili, H. R. Memon, S. R. Samoo, N. H. Mirjat, and K. Harijan, "Overcoming electricity crisis in pakistan: A review of sustainable electricity options," *Renewable and Sustainable Energy Reviews*, vol. 72, pp. 734–745, 2017.

[2] G. W. Hart, "Nonintrusive appliance load monitoring," *Proceedings of the IEEE*, vol. 80, no. 12, pp. 1870–1891, 1992.

[3] F. Zhang, T.-Y. Wu, Y. Wang, R. Xiong, G. Ding, P. Mei, and L. Liu, "Application of quantum genetic optimization of lvq neural network in smart city traffic network prediction," *IEEE Access*, vol. 8, pp. 104 555–104 564, 2020.

[4] T.-Y. Wu, A. Shao, and J.-S. Pan, "Ctoa: Toward a chaotic-based tumbleweed optimization algorithm," *Mathematics*, vol. 11, no. 10, p. 2339, 2023.

[5] T.-Y. Wu, H. Li, and S.-C. Chu, "Cppe: An improved phasmatodea population evolution algorithm with chaotic maps," *Mathematics*, vol. 11, no. 9, p. 1977, 2023.

[6] L. Kang, R.-S. Chen, N. Xiong, Y.-C. Chen, Y.-X. Hu, and C.-M. Chen, "Selecting hyper-parameters of gaussian process regression based on non-inertial particle swarm optimization in internet of things," *IEEE Access*, vol. 7, pp. 59 504–59 513, 2019.

[7] L. Kang, R.-S. Chen, Y.-C. Chen, C.-C. Wang, X. Li, and T.-Y. Wu, "Using cache optimization method to reduce network traffic in communication systems based on cloud computing," *IEEE Access*, vol. 7, pp. 124 397–124 409, 2019.

[8] C.-M. Chen, L. Chen, Y. Huang, S. Kumar, and J. M.-T. Wu, "Lightweight authentication protocol in edge-based smart grid environment," *EURASIP Journal on Wireless Communications and Networking*, vol. 2021, pp. 1–18, 2021.

[9] T.-Y. Wu, Y.-Q. Lee, C.-M. Chen, Y. Tian, and N. A. Al-Nabhan, "An enhanced pairing-based authentication scheme for smart grid communications," *Journal of Ambient Intelligence and Humanized Computing*, pp. 1–13, 2021.

[10] B. Liu, W. Luan, J. Yang, and Y. Yu, "The balanced window-based load event optimal matching for nilm," *IEEE Transactions on Smart Grid*, vol. 13, no. 6, pp. 4690–4703, 2022.

[11] X.-P. Deng, G.-Q. Zhang, Q.-L. Wei, W. Peng, and C.-D. Li, "A survey on the non-intrusive load monitoring," *Acta Automatica Sinica*, vol. 48, no. 3, pp. 644–663, 2022.

[12] M. Afzalan, F. Jazizadeh, and J. Wang, "Self-configuring event detection in electricity monitoring for human-building interaction," *Energy and Buildings*, vol. 187, pp. 95–109, 2019.

[13] Y. Xiao, Y. Hu, H. He, D. Zhou, Y. Zhao, and W. Hu, "Non-intrusive load identification method based on improved km algorithm," *IEEE Access*, vol. 7, pp. 151 368–151 377, 2019.

[14] J.-S. Pan, X.-X. Sun, S.-C. Chu, A. Abraham, and B. Yan, "Digital watermarking with improved sms applied for qr code," *Engineering Applications of Artificial Intelligence*, vol. 97, p. 104049, 2021.
[15] H.-Y. Cui, J. Cai, L. Chen, C. Jiang, Y.-H. Jiang, and X. Zhang, "Non-intrusive load fine-grained identification method based on color encoding," *Power System Technology*, no. 004, p. 046, 2022.
[16] H. Ding, L. Yang, H.-L. Shi, and H. Sun, "Realize intelligent non-intrusive load identification by using data visualization," *Huazhong University of Science and Technology (NATURAL SCIENCE Edition)*, no. 010, p. 049, 2021.
[17] H. Ismail Fawaz, B. Lucas, G. Forestier, C. Pelletier, D. F. Schmidt, J. Weber, G. I. Webb, L. Idoumghar, P.-A. Muller, and F. Petitjean, "Inceptiontime: Finding alexnet for time series classification," *Data Mining and Knowledge Discovery*, vol. 34, no. 6, pp. 1936–1962, 2020.
[18] R. Chu, P. Schweitzer, and R. Zhang, "Series ac arc fault detection method based on high-frequency coupling sensor and convolution neural network," *Sensors*, vol. 20, no. 17, p. 4910, 2020.
[19] Y. Sun, J. Gao, R. Chen, D. Li, L. Yan, X. Cheng, and J. Liu, "Effects of short pulse on lateral current spreading in turn-on process of pulsed thyristors under inductive load," *IEEE Transactions on Plasma Science*, 2023.
[20] Z. Zhao, W. Lu, P. Davari, X. Du, H. H.-C. Iu, and F. Blaabjerg, "An online parameters monitoring method for output capacitor of buck converter based on large-signal load transient trajectory analysis," *IEEE Journal of Emerging and Selected Topics in Power Electronics*, vol. 9, no. 4, pp. 4004–4015, 2020.
[21] F. Jazizadeh, M. Afzalan, B. Becerik-Gerber, and L. Soibelman, "Embed: A dataset for energy monitoring through building electricity disaggregation," in *Proceedings of the Ninth International Conference on Future Energy Systems*, 2018, pp. 230–235.
[22] S. Dargan, M. Kumar, M. R. Ayyagari, and G. Kumar, "A survey of deep learning and its applications: a new paradigm to machine learning," *Archives of Computational Methods in Engineering*, vol. 27, pp. 1071–1092, 2020.
[23] L. Kang, P. Ye, Y. Li, and D. Doermann, "Convolutional neural networks for no-reference image quality assessment," in *Proceedings of the IEEE Conference on Computer Vision and Pattern Recognition (CVPR)*, 2014, pp. 1733–1740.
[24] Y. Gao, O. Beijbom, N. Zhang, and T. Darrell, "Compact bilinear pooling," in *Proceedings of the IEEE Conference on Computer Vision and Pattern Recognition (CVPR)*, 2016, pp. 317–326.
[25] Q. Xu, M. Zhang, Z. Gu, and G. Pan, "Overfitting remedy by sparsifying regularization on fully-connected layers of cnns," *Neurocomputing*, vol. 328, pp. 69–74, 2019.
[26] H. Bao, S. Yang, and Z. Chen, "Review on event inspection based non-intrusive load monitoring algorithms," *Automation of Electric Power Systems*, 2023.
[27] N. Batra, A. Singh, and K. Whitehouse, "Neighbourhood nilm: A big-data approach to household energy disaggregation," *arXiv preprint arXiv:1511.02900*, 2015.
[28] C. C. Yang, C. S. Soh, and V. V. Yap, "A non-intrusive appliance load monitoring for efficient energy consumption based on naive bayes classifier," *Sustainable Computing: Informatics and Systems*, vol. 14, pp. 34–42, 2017.
[29] L. Du, Y. Yang, D. He, R. G. Harley, T. G. Habetler, and B. Lu, "Support vector machine based methods for non-intrusive identification of miscellaneous electric loads," in *IECON 2012-38th Annual Conference on IEEE Industrial Electronics Society.* IEEE, 2012, pp. 4866–4871.
[30] Y.-X. Lai, C.-F. Lai, Y.-M. Huang, and H.-C. Chao, "Multi-appliance recognition system with hybrid svm/gmm classifier in ubiquitous smart home," *Information Sciences*, vol. 230, pp. 39–55, 2013.